The microstructure and microchemistry of synthetic zirconolite, zirkelite and related phases

Timothy J. White

School of Science, Griffith University
Nathan, Queensland, 4111, Australia

Abstract

An alternative description of zirconolite, zirkelite, pyrochlore and polymignyte as modular structures is proposed. This approach not only emphasizes their crystallographic similarities but is also readily extended to include "defects" which were observed by high resolution electron microscopy. Each module consists of two layers of octahedrally coordinated cations (Ti, Ta, Nb) arranged as an hexagonal tungsten bronze (HTB) type motif. The interstice formed by the six-membered octahedral ring is occupied by a REE/ACT atom in 8-fold coordination or a transition metal atom accommodated statistically in either tetrahedral or trigonal bipyramidal sites. Interlayer cations are in cubic (Ca, Na, REE, ACT), monocapped octahedral (Zr) or octahedral (Ti, Ta, Nb) coordination. Every HTB layer is displaced with respect to those immediately adjacent by an interlayer stacking vector whose magnitude and direction may be varied to derive the various structures. Thus the structures may be regarded as polytypic; the simplest member (i.e., the aristotype) is zirconolite. Because the HTB layers possess (pseudo) hexagonal symmetry subsequent modules are related to each other by $-n\pi/3$ rotations. The description is conveniently simplified by considering the cation net of each HTB layer, the nodes of which correspond to the kagomé net. Polymignyte is composed of slightly different modular units in which the layer cations are arranged as intergrowths of the kagomé net and a distorted triangular net.

The justification for this approach was confirmed by examining zirconolite, doped with Mg, Al, REE, ACT and various transition metal elements, by high resolution electron microscopy and analytical electron microscopy. At low concentrations—the exact level was dependent upon the element(s)—the dopants were accommodated as dilute solid solutions; i.e., isomorphic substitutions. Incorporation of higher dopant concentrations led to polysynthetic twinning on [130], [$\bar{1}$30] and [010] twin axes; on occasion the twinning was completely regular and new polytypes resulted. At sufficiently high concentrations of REE/ACT pyrochlore was stabilized in favor of zirconolite. Coupled ACT/Mg, Al, Fe substitutions yielded zirkelite and polymignyte. Since the minerals have stability fields which are composition dependent they cannot strictly be regarded as polytypic and are best considered as pseudotypes.

Introduction

Although the structure of pyrochlore has been known for some time (Strukturbericht, 1914; Gaertner, 1930) those of zirconolite (Rossell, 1981; Gatehouse et al., 1981), zirkelite and polymignyte (Mazzi and Munno, 1983) have only recently been determined. Indeed for many years there was considerable confusion as to the identity of these structures and the minerals were often regarded as isotypes (Hussak and Prior, 1895; Blake and Smith, 1913; Lima-de-Faria, 1958; Pyatenko and Pudovkina, 1964; Hogarth, 1977). This ambiguity was principally due to the propensity of these minerals to accommodate the radionuclides $^{238}_{92}U$, $^{235}_{92}U$ and $^{232}_{90}Th$; these isotopes are the parents of the three natural disintegration series involving α and β emission. Thus X-ray crystallographic studies were hampered because the accumulated radiation dose resulted in either partial or complete metamictization.

It is appropriate, in view of our newly acquired appreciation for these structures, to review the underlying crystallographic similarities of the minerals and examine the physical and chemical conditions which give rise to the characteristic pseudotypic modifications.

Structural relationships

Previous studies

Pyrochlore, zirconolite, zirkelite and polymignyte are anion-deficient superstructures of the fluorite type with

the ideal stoichiometry $A_2B_2X_7$ (A = Ca, Na, REE, ACT, Zr, Ti; B = Ti, Nb, Ta, Al, Fe; X = O,F). The pyrochlore structure is the most thoroughly studied of these and has been described in a variety of ways. Sleight (1969) considered it to be a pair of interpenetrating B_2X_6 and A_2X (anticristobalite) nets, while Pannetier and Lucas (1970) utilized the $B_4\square$ (cristobalite) and A_2X networks. Alternatively pyrochlore can be related to $AgSbO_3$ or $MgCu_2$ (Bagshaw, 1976). These descriptions are reviewed by Subramanion et al. (1983). Mazzi and Munno (1983) derived polymignyte, zirconolite and zirkelite from pyrochlore by interchanging chains of like cations among the four structures. It has been noted that both pyrochlore (Derriet et al., 1971; Yagi and Roth, 1978; Nyman, 1983) and zirconolite (Rossell, 1981) possess BX_6 arrays arranged as hexagonal tungsten bronze (HTB) motifs.

Modular structure building principle

In this paper we outline an approach that quite naturally takes into account the layered nature of the structures, supplies a simple interpretation of "defects" observed by high resolution transmission electron microscopy (HRTEM) and is equally applicable to other members of the group that were identified during this study.

We have previously described zirconolite as the aristotype of a structural family (White et al., 1984) whose members are constructed by stacking modular units in a variety of orientations. Each module consists of two HTB layers and the interposed cations (Fig.1). The layers are displaced with respect to each other by an *interlayer stacking vector* (SV) which is defined as the projected distance, viewed down the (pseudo) six-fold axis, between crystallographically similar atoms in adjacent layers. The angle between successive stacking vectors is the *intermodular stacking angle* (SA) and can take any $-n\pi/3$ value. Each layer belongs to a region of lattice coincidence between adjacent modules; hence in a repeat sequence the number of layers must be equivalent to the number of modules. In zirconolite itself successive modules are related to each other by a SA of $-180°$. The orientation relationships are such that the insertion of SA's of $-120°$ and $-300°$ result in a [130] twin, while a SA of $-60°$ or $-240°$ leads to a [$\bar{1}$30] twin. A SA of $-360°$ yields a twin on [010]. It was proposed that a family of polytypes could be generated by the regular insertion of twin planes on a unit cell scale. This structure building principle is completely analogous to that used to describe the mica polytypes (Smith and Yoder, 1954; Thompson, 1981).

To facilitate the direct comparison of zirconolite and its related structures we adopt the non-standard c-centered unit cells used by Mazzi and Munno (1983) (Table 1); these relationships are shown schematically in Figure 2. In all cases the $(001)_c{}^1$ basal plane is coincident with the
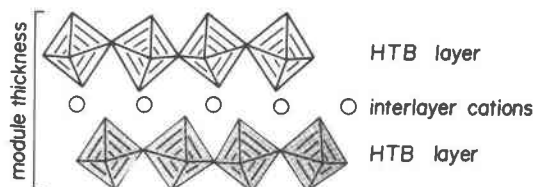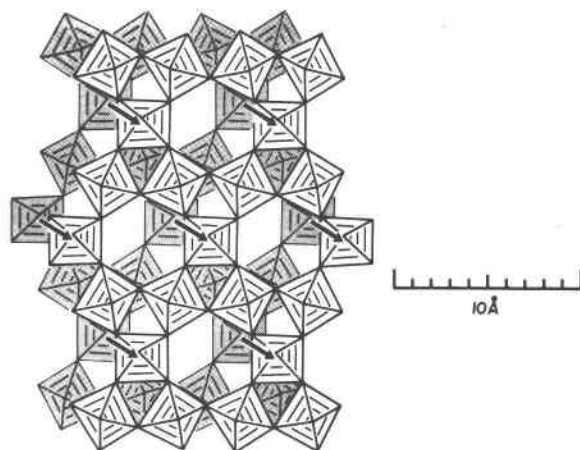
^{1} Subscripts c, cu, o, t refer to c-centred, cubic, orthorhombic and trigonal axial settings.

Fig. 1. (a) Two *HTB* layers, ie. one module, as they occur in zirconolite and its polytypes. The lower layer is offset from the upper by an interlayer stacking vector (arrowed). (b) The *HTB* layers viewed from the side showing the placement of interlayer cations.

HTB layers; different modular stacking sequences give rise to different c^* translational periodicities.

Zirconolite

The *HTB* layers of zirconolite are related by a SV of magnitude 2.1Å whose direction alternates between the $[130]_c$ and $[\bar{1}30]_c$. This yields a bimodular repeat with $c^* = 11.15$Å. The most common cation of the HTB layers is Ti however Nb-rich varieties have been reported (Borodin et al., 1961). The large interstice of the HTB layer is occupied by Ti atoms which are statistically distributed over two 5-coordinate trigonal bipyramidal sites (Figs. 3a,b). In the interlayer region like cations form strings of distorted cubes (Ca, REE, ACT) or face-capped octahedra (Zr) which run parallel to $[110]_c$ and $[\bar{1}10]_c$ directions in alternate cation planes (Fig. 3c).

Zirkelite

The modules of zirkelite are almost identical to those found in zirconolite (Fig. 4a,b) however the SV propogate in a cyclic manner in the $[130]_c = [120]_t$, $[\bar{1}30]_c = [110]_t$ and $[100]_c = [210]_t$ directions to yield a trimodular repeat. Consequently, chains of identical interlayer cations run

Table 1. Unit cell parameters for zirconolite, pyrochlore, zirkelite and polymignyte

				Standard setting			
Mineral	$a(\overset{\circ}{A})$	b	c	$\alpha(°)$	β	γ	Ref.
Zirconolite	12.611	7.311	11.444	90	100.52	90	1
Pyrochlore	10.2978	10.2978	10.2978	90	90	90	2
Zirkelite	7.287	7.287	16.886	90	90	120	2
Polymignyte	10.148	14.147	7.278	90	90	90	2

				C-centered cell			
Mineral	$a(\overset{\circ}{A})$	b	c	$\alpha(°)$	β	γ	Ref.
Zirconolite	12.611	7.311	11.444	90	100.52	90	1
Pyrochlore	12.61	7.26	17.84	90	90	90	2
Zirkelite	12.62	7.29	16.89	90	90	90	2
Polymignyte	2x12.37	7.28	17.41	90	90	90	2

Reference 1 Gatehouse *et al.*, 1982.

          2 Mazzi & Munno, 1983.

parallel to $[010]_c = [010]_t$, $[110]_c = [110]_t$ and $[1\bar{1}0]_c = [100]_t$ (Fig. 4c).

Pyrochlore

Pyrochlore possesses four $[111]_{cu}$ HTB BO_6 planes. The displacement between successive HTB layers is $2 \times 2.1Å$ along $[130]_c = [2\bar{4}1]_{cu}$, $[\bar{1}30]_c = [4\bar{2}1]_{cu}$ and $[\bar{1}00]_c = [\bar{1}11]_{cu}$. This results in a trimodular repeat with c^* equal to 17.84Å (Fig. 5a,b). In this instance the HTB layers may contain substantial amounts of Nb and Ta as well as Ti. The interstice formed by the six-membered octahedral ring is occupied by a large A cation in eight-fold coordination; the $A(O_6F_2)$ polyhedron may be considered as a distorted cube or alternatively can be described as a puckered hexagonal bipyramid (Nyman et al., 1978). The interlayer cations (Fig. 5c) consist of strings of AX_8 polyhedra which alternate with AX_8/BO_6 chains in the $[110]_c$, $[1\bar{1}0]_c$ and $[010]_c$ directions.

Polymignyte

Polymignyte contains layers which are substantially of the HTB type but differ from the aristotype by containing $(100)_c$ shear planes (Fig. 6a). The structure is simply derived from HTB by replacing every second $\square X_8/BX_6$

polyhedral string by chains of ZrO_7 edge-capped octahedra. The remaining six-membered BX_6 octahedral rings contain Fe distributed statistically over tetrahedral and trigonal bipyramidal sites.

Although the modules of polymignyte differ from those previously encountered the same descriptive principle applies. Each module contains two modified HTB layers offset by a SV of 5.5Å along $[\bar{1}30]_c = [213]_o$; a trimodular repeat results (Fig. 6b). The interlayer cations occur as chains of AO_8 distorted cubes, AO_7 monocapped octahedra and BO_6/FeO_5, FeO_4 polyhedra which run parallel to $[010]_c$ (Fig. 6c).

A concise description using cation nets

Since the cation array of the fluorite substructure is hardly distorted, (the (111) planes of CaF_2 correspond to the $(001)_c$ planes), it is possible to consider the displacements between the nodes of the cation net just as we have done for the HTB layers. This has the advantage that the layers may be illustrated more concisely and the relationship between SV more easily recognized.

The correspondence between an HTB layer of pyrochlore and its cation sublattice is illustrated in Figure 7a; this arrangement is known as the kagomé net (O'Keeffe and Hyde, 1981). (If the large cation or statistical cation pair were included an almost perfect triangular net would result (Fig. 7a)). For polymignyte the incorporation of ZrO_7 polyhedra yields a net which is an intergrowth between the kagomé and distorted triangular nets (Fig. 7b). The (shortest) displacement in projection between like atomic nodes is the SV for the polytype; the angle between SV is the SA. The displacements between the cation nets in all four structures are shown in Figure 8.
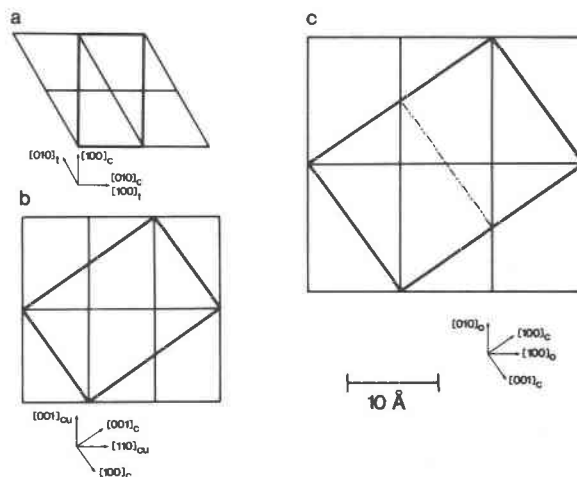

Fig. 2. A schematic illustration showing the relationships between the C-centered cells (thick lines) and the standard settings (light lines) of (a) trigonal zirkelite, (b) cubic pyrochlore and (c) orthorhombic polymignyte.
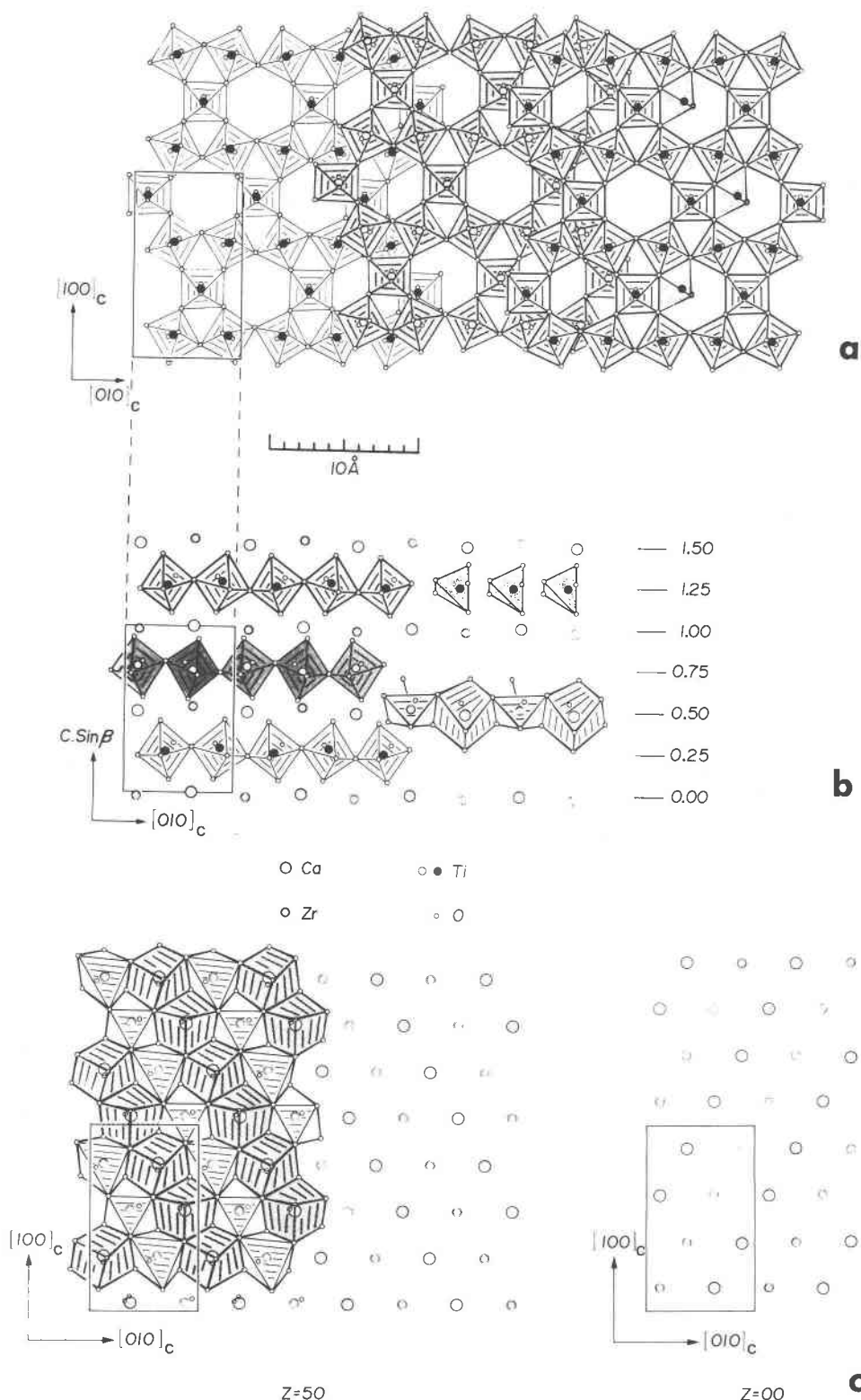
Fig. 3. (a) The zirconolite structure projected down c*. TiO$_6$ octahedra are arranged in an *HTB* type motif; the unshaded layers on the extreme left and right are equivalent and correspond to the lower most and uppermost layers respectively. The stippled polyhedra in the six-membered octahedral rings represent one of a statistical pair of TiO$_5$ trigonal bipyramids. (b) The [100]$_c$ projection. On the left TiO$_6$ octahedra at z = ±0.25 are emphasized; on the right some of the distorted CaO$_8$ cubes, ZrO$_7$ faced-capped octahedra and TiO$_5$ trigonal bipyramids are shown. (c) The polyhedra of the interlayer cation planes. Strings of CaO$_8$ cubes alternate with chains of ZrO$_7$ face-capped octahedra. These run parallel to [1$\bar{1}$0]$_c$ and [110]$_c$ at z = 50 and z = 0 respectively. (Gatehouse et al., 1981).
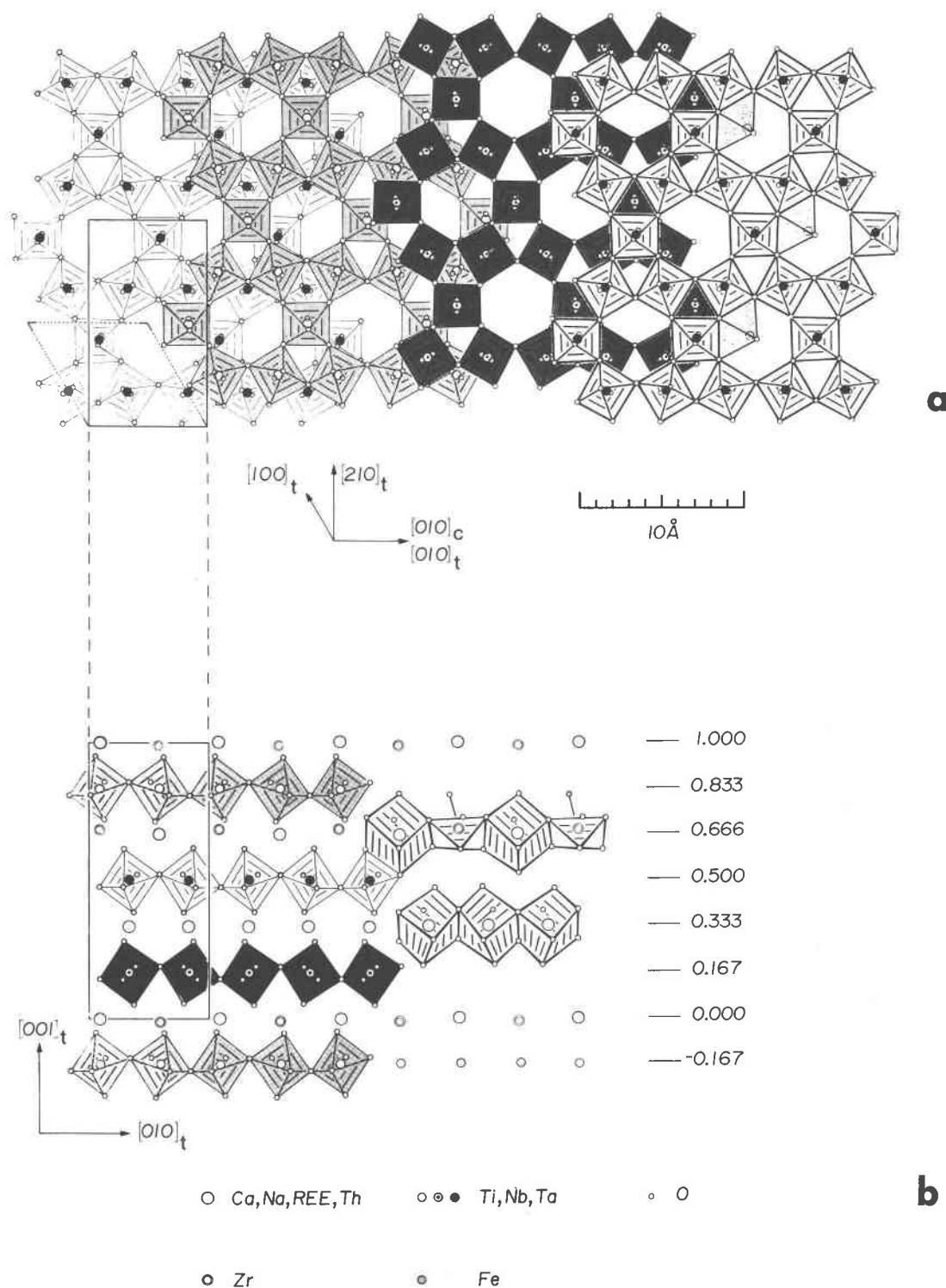
Fig. 4. The zirkelite structure showing: (a) The *HTB* arrays of (Ti, Nb, Ta) O$_6$ octahedra viewed along c*. Three FeO$_5$ trigonal bipyramids are emphasised on the right hand *HTB* layer. (b) The [100]$_c$ = [001]$_t$ projection showing octahedral layers at z = 0.167, 0.500 and 0.833. On the right AO$_8$ polyhedra and AO$_7$ monocapped octahedra are illustrated. (c) The interlayer polyhedra. Strings of like cations run parallel to the [010]$_c$ = [010]$_t$ [1$\bar{1}$0]$_c$ = [100]$_t$ and [110]$_c$ = [110] directions at z = 0.333, 0.666 and 0.000 respectively (Mazzi and Munno, 1983).

$z = 0.33$ $z = 0.66$ $z = 0.00$

$[100]_t$ $[210]_c$

$[010]_c$ $[010]_t$

10Å

c
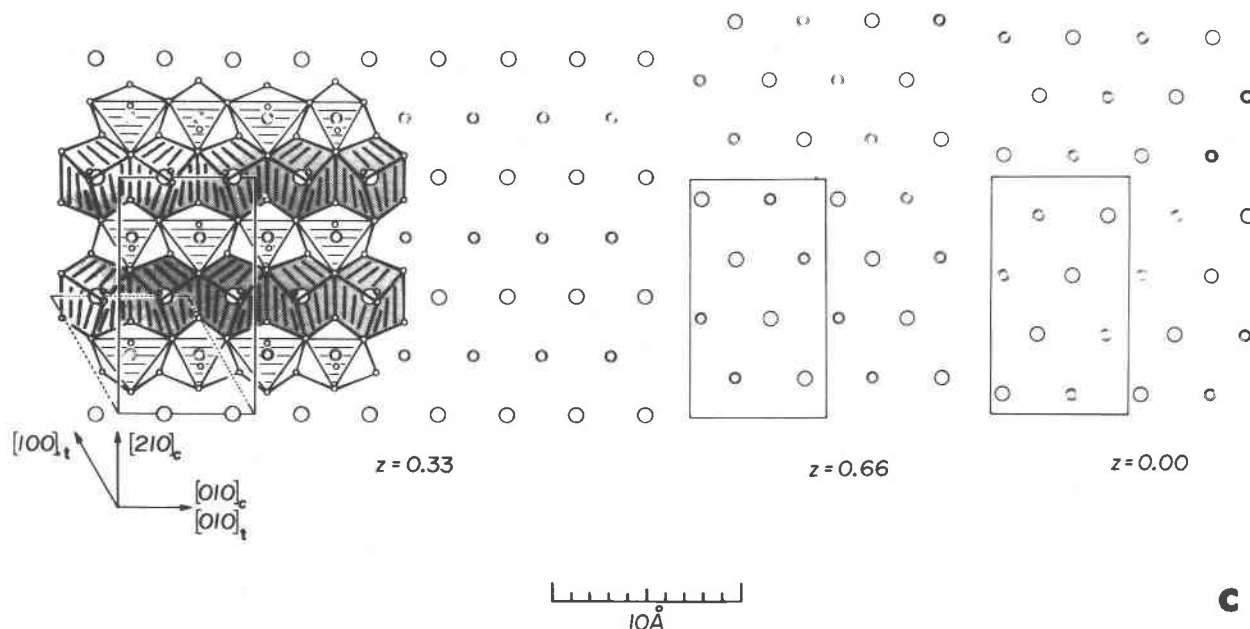
Similarities between the zirconolite group and mica polytypes

It was pointed out previously that the modular description used here is very similar to that employed to emphasize similarities among the mica polytypes. These structures can be usefully represented by stacking vector diagrams in which the SV's are projected upon the basal plane. A crystallographic repeat is obtained when a sequential plot of SV's either returns to the start of the plot or finishes on a c-center. These diagrams plainly illustrate the relationships between the hettotypes and the way in which twin boundaries may be considered as very narrow lamellar intergrowths of other polytypes.

The SV diagrams for zirconolite, zirkelite, pyrochlore and polymignyte are shown in Figure 9; in addition the twin laws operating in zirconolite are given. Inspection of these figures clearly shows that a t-type boundary in zirconolite is equivalent to a lamellar defect of zirkelite and that an m-type twin results in a displacement between alternate HTB layers which is equal to the displacement between successive layers in pyrochlore.

Polytype (pseudo-type) symbols

For those pseudotypes with modules of the same form (i.e., zirconolite, zirkelite, pyrochlore) the SV is $(2 \times)2.1$Å; this is the *unit displacement*. The SA's $-n\pi/3$, with n = 1,2,3,4,5,6 are given the symbols h, t, d, t_2, h_5 and m respectively (White et al., 1983; Thompson, 1981). Thus a polytype symbol of the general form $(\pm mr)^n$ can be given where $\pm m$ is the number of unit SV displacements in an arbitrarily chosen direction, r is the SA, and n is the number of modules in the crystallographic repeat. Zirconolite for example contains SV's of unit displace-

ment which alternate between the $\pm[130]$ directions and are related by an intermodular SA of $-\pi$; therefore its modular stacking sequence is . . . $d - d$ $(d - d)$ $d - d$ . . . $= (d–d)$. Round brackets delineate the *crystallographic repeat* which may or may not be equivalent to the *formula repeat*. Pyrochlore contains SV displacements which are two units in length and related to each other by SA's of $-2\pi/3$. Therefore its symbol is . . . $2t$ $(2t$ $2t$ $2t)$ $2t$ . . . $= (2t)^3$; on this occasion the formula repeat is $2t$ and the crystallographic repeat $(2t)^3$.

Polymignyte, because its modules are of a different form uses a SV whose (unit) magnitude is 5.5Å. The SA is -2π and its modular stacking sequence is . . . $m(m$ m $m)m$ . . . $= (m)^3$.

A summary of relevant polytype formula is given in Table 2.

Experimental procedures

Specimens were prepared at the compositions, temperatures and pressures summarized in Table 3. Most samples were obtained from Professor A.E. Ringwood's group at A.N.U. and had previously been studied by electron probe microanalysis and Guinier powder X-ray diffraction (Sinclair, 1982; Kesson et al., 1984).

The samples were prepared by crushing under ethanol and depositing on holey carbon grids in the usual way. High resolution electron microscopy (HRTEM), analytical electron microscopy (AEM) and selected area diffraction (SAD) were carried out on JEOL 100C microscopes operated at 100 keV. To permit the direct observation of any order-disorder phenomena along c^*, images were recorded in the $[010]_c$, $[110]_c$ or $[130]_c$ orientations. Beam damage was minimal except in those instances where the U content was high; such specimens melted rapidly under the converged electron beam. Energy dispersive X-ray analyses were obtained from crystal fragments which had
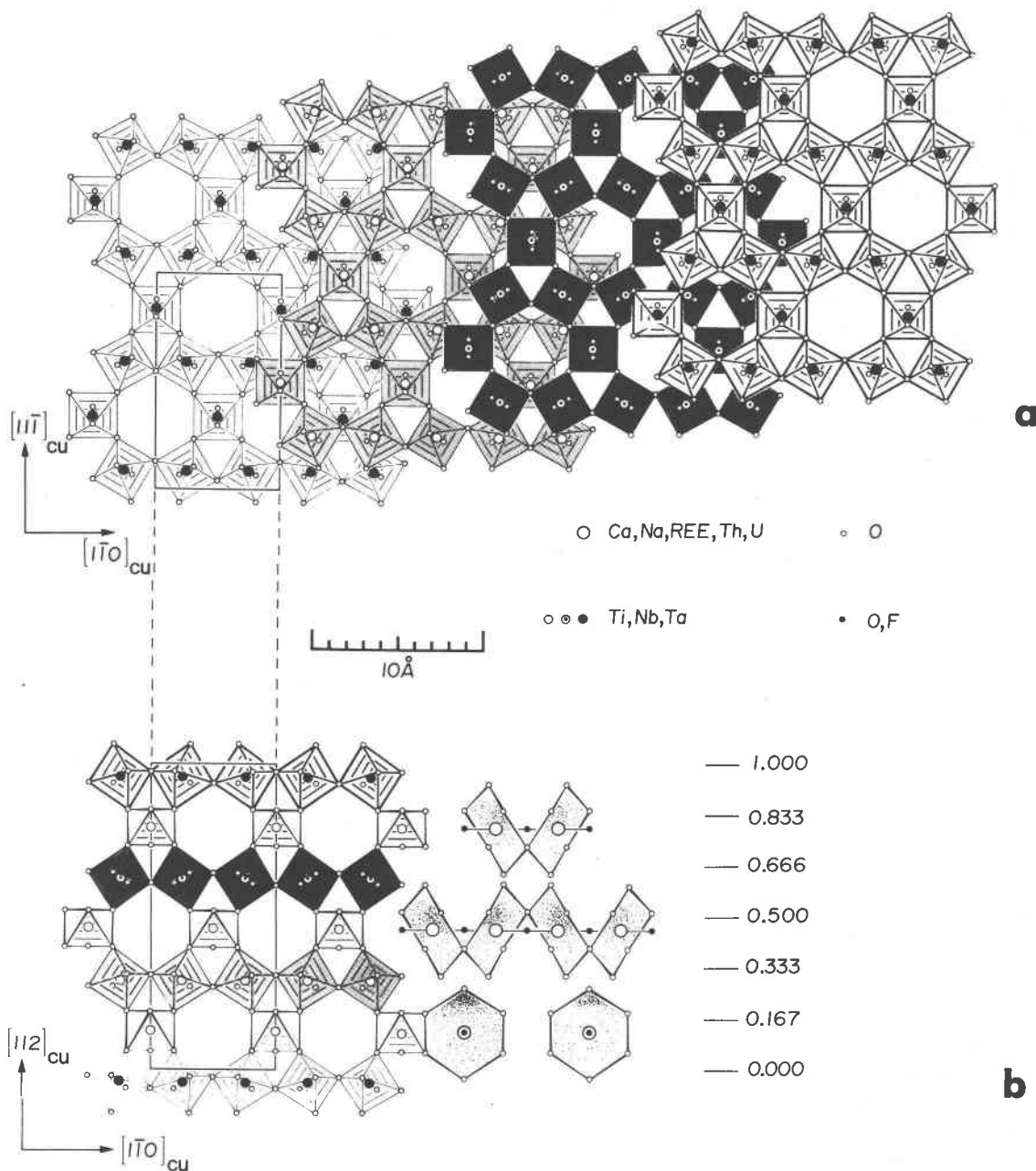
Fig. 5. (a) The pyrochlore structure projected down $[001]_c = [110]_{cu}$ emphasizing the *HTB* layers. (b) The $[100]_c = [11\bar{1}]_{cu}$ projection. *HTB* layers occur at z = 0.292, 0.625 and 0.958. (c) An interlayer region containing A (O_6F_2) puckered hexagonal bipyramids and BO_6 octahedra. On the right the correspondence between the bipyramid and a distorted cube is shown (Mazzi and Munno, 1983).

previously been identified by SAD; background peaks of Cu, Sn and Zn were always present. No attempt was made to quantify these analyses.

Image interpretation

Images consisted of fringes ~5.6Å wide that were interpreted as being due to the modular units; translational periodicity across these fringes which arose from differences in contrast was taken to be the crystallographic repeat. Attempts to calculate images for zirconolite in this and other laboratories have met with mixed success (Hutchison et al., 1983); although the gross features with which we are concerned are correct, finer detail has not been successfully matched. This problem is exacerbated in crystals containing significant amounts of heavy REE or ACT elements.
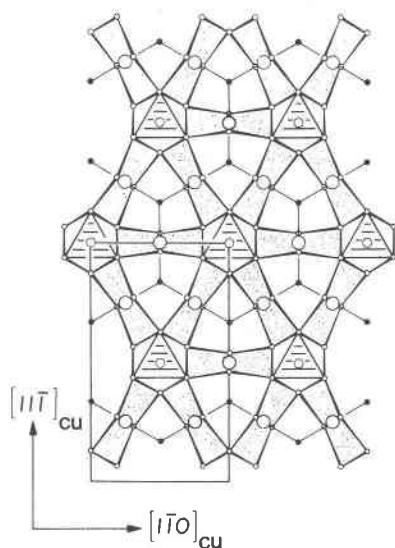
Twinned zirconolite

We reported elsewhere (White et al., 1984) that zirconolite, a component of SYNROC, a titanate ceramic designed to immobilize high level nuclear waste (Ringwood et al., 1981), was often twinned on a unit cell scale. Significantly, stoichiometric and non-stoichiometric zirconolite preparations which (nominally) only contained Ca, Ti and Zr oxides never exhibited the twinning phenomenon (see Table 3). Therefore, it was clear that certain components of the simulated radwaste were responsible for these structural modifications. Additionally, it could reasonably be inferred that these were incorporated on the twin boundaries.

SAD was used to examine "zirconolites" which had been doped with a number of elements as this technique could be used to rapidly identify twinned crystallites (White et al., 1984). The elements Al, Ce, Nd, Sm, Gd, Yb, Th and U were found to promote twinning (Fig. 10a). The elemental concentration at which zirconolite became saturated and started to twin varied considerably. For example, Al^{3+} (CR = 0.67Å) which substitutes for Ti^{4+}/Ti^{3+} (CR = 0.745Å/0.81Å) induces twinning at quite low levels.[2] Th and the REE partition into the Ca (1.26Å) sites while U replaces Zr (0.92Å) (Kesson et al., 1984). Twinned crystallites could be detected in all REE/ACT-doped preparations however the small heavy REE Yb(1.12Å) were less likely to cause twin behavior than the larger light REE's, viz. Ce (1.28Å), Nd (1.26Å), Sm (1.23Å), Gd (1.20Å), or the actinides, viz. U (1.14Å) and Th (1.20Å).

Elements which are apparently incorporated in zirconolite by isomorphic substitution are Fe(CR = 0.75Å) and Mn(1.07Å); however, the iron result should be treated cautiously since it was observed only as an "impurity" cation in the zirconolite preparation and its concentration was quite low.

Although no attempt was made to quantify the spectra it was obvious that within each sample there were considerable compositional differences between grains. In particular the Zr concentration could be extremely variable. The fact that the zirconolite structure is not disrupted suggests that substantial amounts of

[2] All crystal radii (CR) from Shannon and Prewitt (1969).
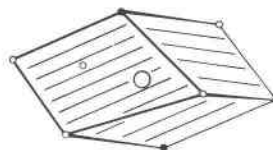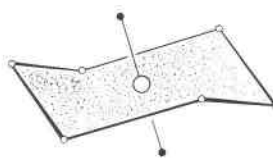
Zr can be replaced by Ti. No correlation between the zirconium concentration and the frequency of twinning could be recognised.

A typical twinned zirconolite crystallite is shown in Figure 11; alternating dark and light bands represent $[1\bar{1}0]_c$ and $[010]_c$ orientations respectively. The boxed area contains what appears to be a small region of an $(r)^4$ member intergrown with the $(d-d)$ aristotype.

Zirconolite—zirkelite intergrowths

It was shown earlier that zirconolite and zirkelite are composed of identical modules which are related by SA's of $-180°$ and $-120°$ respectively. Zirkelite may be derived from zirconolite by the mimetic (Hyde et al., 1981) insertion of t-type twin boundaries in the latter structure. Therefore it is not surprising that coherent intergrowths between the two minerals were observed.

Preparations with bulk compositions $Ca_{0.77} Th_{0.24} ZrTi_{1.5} Al_{0.5} O_7$ and $Ca_{0.7} Th_{0.3} Zr Ti_{1.7} Mg_{0.3} O_7$ yielded crystals which consisted almost entirely of perfect $(t)^3$ zirkelite (Fig.10b). A high resolution micrograph of zirkelite and its associated diffraction pattern is shown in Figure 12. The intensity distribution of the second order reflections is unusual as strong spots occur in pairs (arrowed). This would seem to be indicative of twinning, however none of the known twin laws nor intergrowth with zirconolite can account for this phenomenon. It is worth noting that this diffracted intensity was invariant in all the crystallites examined. Coupled Th/Fe substitutions also yielded the $(t)^3$ hettotype however in this instance intergrowth with other $(r)^n$ structures was common. This is illustrated in Figure 13; $(d-d)$ and $(t)^3$ members predominate but a few $(r)^n$, n > 3 repeat units are also present.

Other examples of mimetically twinned intergrowths.

In zirconolite formulations of composition $Ca_{1-x/2}$ REE $Zr_{1-x/2} Ti_2O_7$ 0.25 < x < 1.0 polysynthetic twinning was occasionally perfectly ordered to yield other hettotypes of the zirconolite family. At higher REE concentrations (viz. Sm— "zircono-
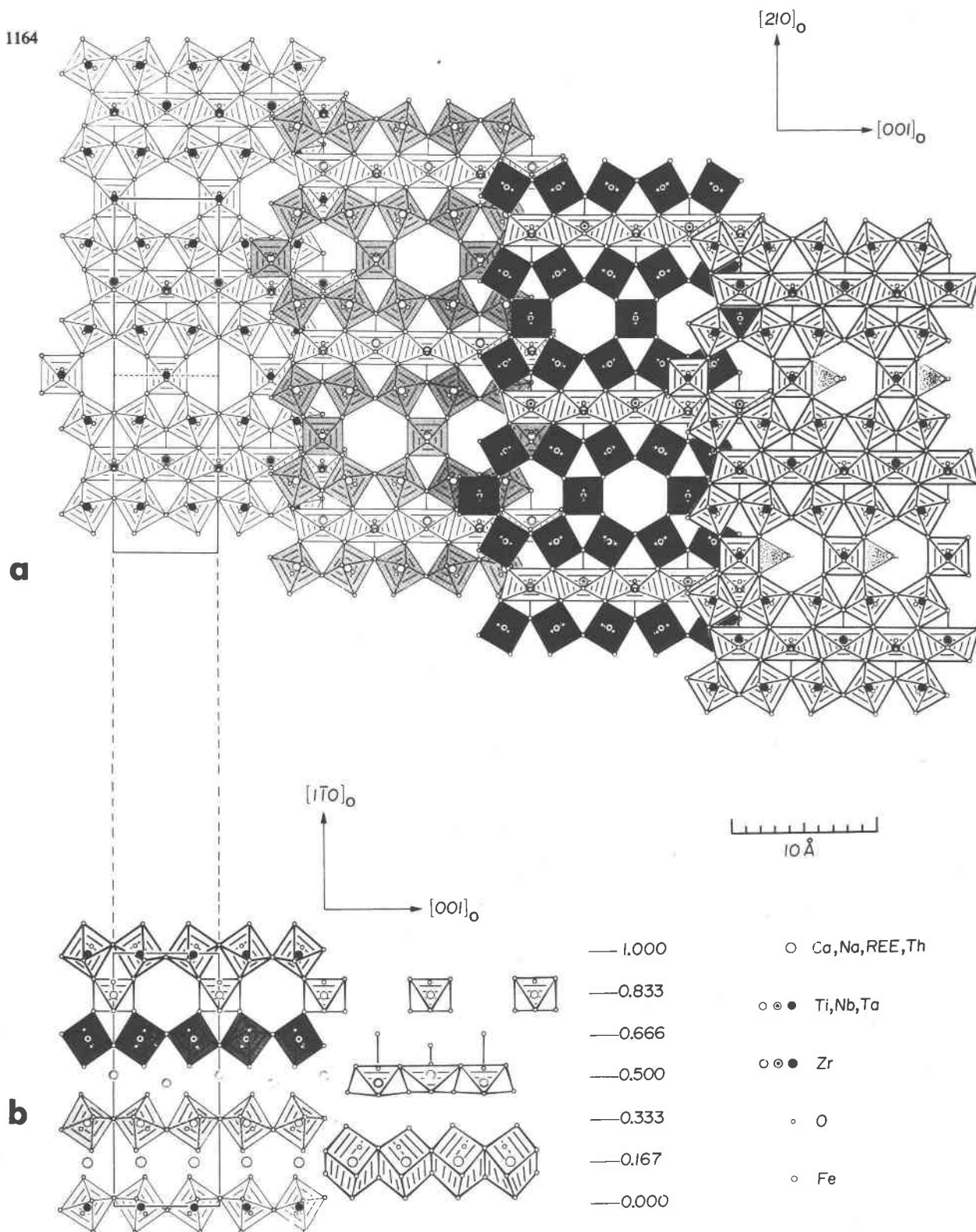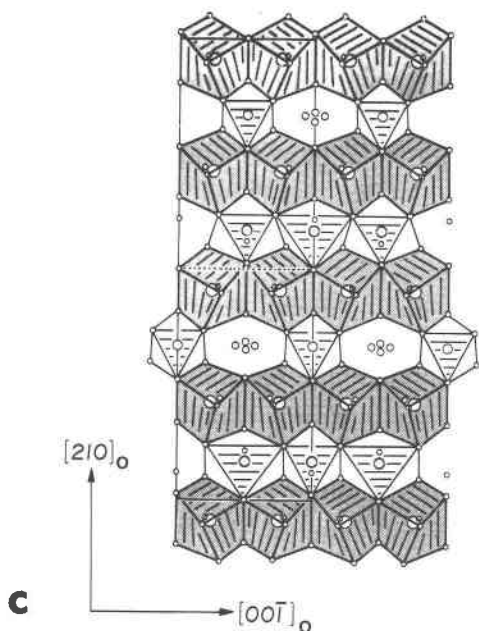
1164

Fig. 6. (a) Polymignyte projected down $[001]_c = [120]_o$. The *HTB* portion of the layers is emphasized; these are separated by $[010]_c = [001]_o$ chains of edge-capped ZrO_7 octahedra. The insertion of these polyhedra yields a basal repeat which is doubled along $[100]_c = [210]_o$. FeO_4 tetrahedra and FeO_5 trigonal bipyramids (not shown) occupy the six-membered octahedral rings in a statistical manner. (b) The $[100]_c = [110]_o$ projection showing the modified *HTB* layers at z = 0.000, 0.333, 0.666. On the right interlayer polyhedra are emphasized, *viz.* BO_6 octahedra, ZrO_7 monocapped octahedra and AO_8 cubes. (c) A plane of interlayer polyhedra. Strings of AO_8 and ZrO_7 polyhedra run parallel to $[010]_c = [001]_o$. As well BO_6 octahedra alternate with FeO_5 polyhedra centered statistically over four sites (Mazzi and Munno, 1983).

$[210]_o$

c

$[00\bar{1}]_o$

ary insertion is compositionally dependent. Consequently, the members are best considered to be pseudotypes.

At "low" concentrations ACT and REE elements are incorporated in zirconolite by isomorphic substitution to yield a dilute solid solution. Other mechanisms become operative at higher concentrations. One involves the incorporation of dopants in the extended defects which result from polysynthetic twinning on [130], [$\bar{1}$30] or [010]. The cation sublattice is essentially undisturbed by these twinning operations; presumably the effect of twinning is to distort the anion array slightly which facilitates the incorporation of other elements. Second, when certain elements are at sufficiently high concentration and/or coupled substitutions are employed mimetic twinning produces $(r)^n$, $n > 2$ hettotypes. The crystal structure of one of these has recently been refined (Munno and Mazzi, 1983) and was shown to be the $(t)^3$ pseudotype. In addition HRTEM revealed an $(r)^4$ type. Unfortunately, at the available resolution it was not possible to unequivocally determine its modular stacking formula; however
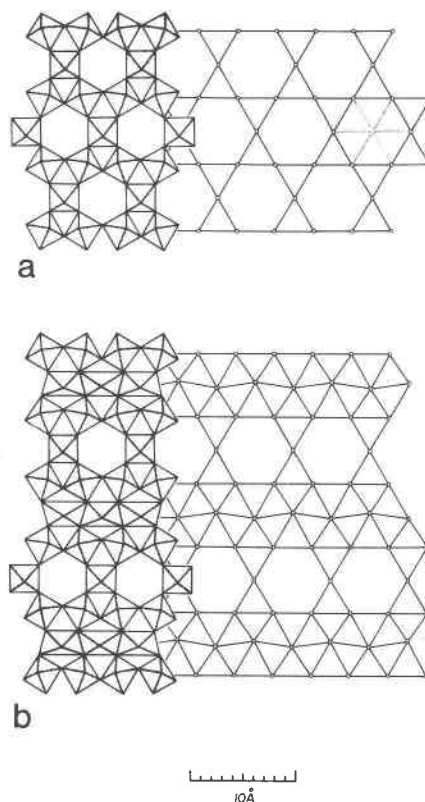
lite", x = 1.0) more complete ordering rarely lead to ordered $(r)^4$ superstructures; the SAD pattern of such a crystallite is shown in Figure 14. Usually though, the $(r)^4$ structure was coherently intergrown with other group members (Fig. 15). Some crystals of the $Ca_{0.87}$ $Nd_{0.26}Zr_{0.87}Ti_2O_7$ sample yielded similar diffraction patterns and images.

Disordered intergrowths

Zirconolites of nominal formulation $CaZrTi_{1.70}Al_{0.30}O_{6.7}$ were prepared under 5 kbar pressure at temperatures of 1250, 1300, and 1400°C. The lower temperature runs yielded zirconolite which was often twinned polysynthetically on $(001)_c$. At higher temperatures the reflections in SAD patterns became more diffuse and complex modular intergrowths were observed. Figure 16 illustrates a crystal in which there is an irregular distribution of $(r)^n$, n = 2,3,4 polytypes.

Pyrochlore and polymignyte

U-pyrochlores of composition CaU_{1-x} Zr_xTi_2 O_7, x = 0.25, 0.5, 0.75 were studied. Unlike the zirconolite–zirkelite samples no twinning or disorder was observed along the modular stacking direction $[112]_{cu}$ (Fig. 17 a,b).

Polymignyte was synthesised from only one composition (viz. $Ca_{0.7}Th_{0.3}ZrTi_{0.7}Fe_{0.3}$ O_7) and was always perfectly crystalline. In Figure 17. c,d its SAD pattern and X-ray spectra are compared with that of pyrochlore.

Discussion

We have previously argued (White et al., 1984) that a polytypic family could be generated by the regular insertion of twin boundaries in zirconolite. These experiments confirm this belief, however, the pattern of twin bound-

a

b

10Å

Fig. 7. (a) The cation nodes of an *HTB* array correspond to a kagomé net. If the cation site at the center of the six-membered ring were occupied a triangular net would result (dotted lines). (b) In polymignyte the cation nodes of the modified *HTB* layer yield a net which is an intergrowth between the kagomé net and a distorted triangular net.
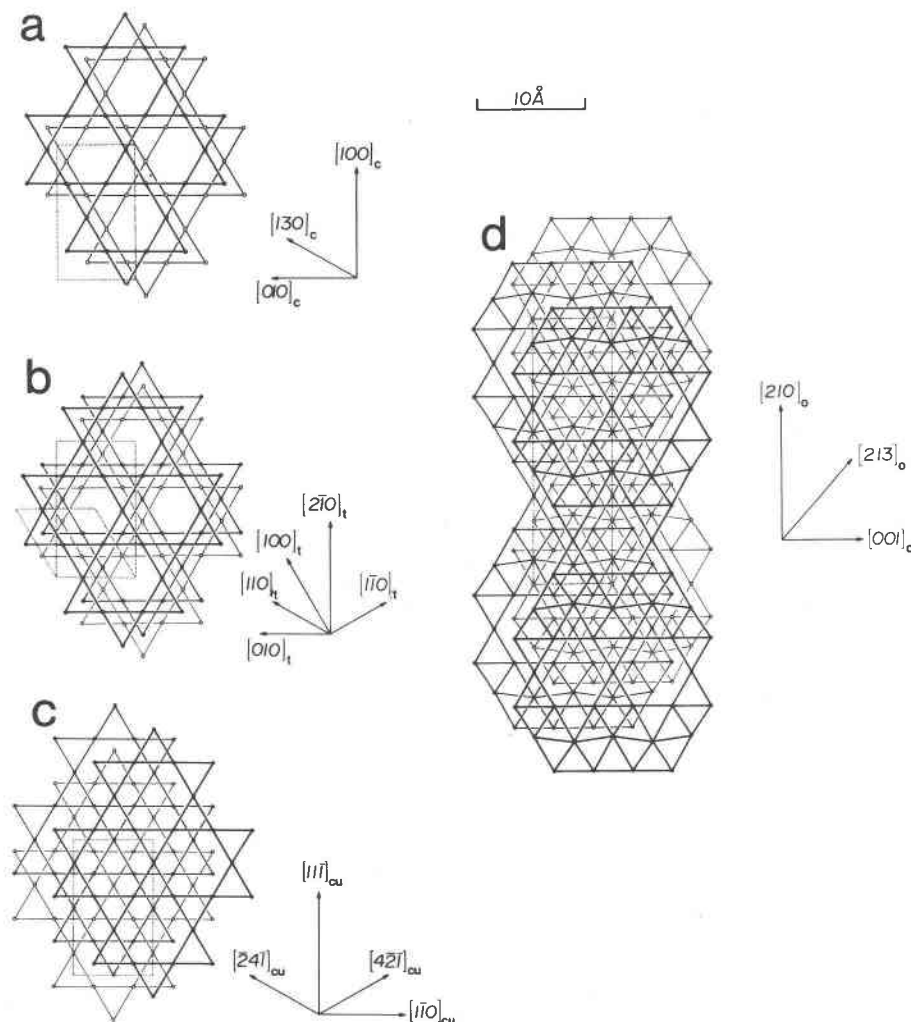
Fig. 8. The displacement between successive cation nets in (a) zirconolite (b) zirkelite (c) pyrochlore and (d) polymignyte. The uppermost layer is drawn in heavy pen, the lower layers more lightly. Nodes are indicated by, (in increasing height), open, half-filled and filled circles.

both $(m)^4$ and $(mdmd)$ types would yield hettotypes with the appropriate c* repeat. Clearly, an infinite number of stacking sequences are possible and future studies may reveal other family members (in much the same way as the number of mica polytypes has gradually increased).

At still higher dopant concentrations the SV is doubled, but continues to operate along the $[130]_c$, $[\bar{1}30]_c$ and $[001]_c$ directions and pyrochlore is produced; disorder arising from polysynthetic twinning was not observed though. When Th/Fe coupled substitutions were employed polymignyte was synthesised. Structurally, it is closely related, but quite distinct from zirconolite, zirkelite and pyrochlore. Its modules contain layers in which the HTB portions have been sheared to incorporate ZrO_7 polyhedra. Once again no disorder was detected.

Thus, polysynthetic twinning of zirconolite due to high actinide/rare earth concentrations preempts the formation of pyrochlore and polymignyte. However, the extent of order/disorder is also dependent upon the temperature of preparation as exemplified by the Al-doped zirconolites. At higher preparative temperatures a variety of $(r)^n$ structures are produced, but they are only one or two unit cells in extent.

Our results are in agreement with the microprobe data of Kesson et al. (1984) which suggest that the crystal chemistry of the REE in zirconolite is variable. Single element rare earth dopings showed the tolerance of zirconolite for Yb to be greater than for Nd and Gd. Approximately 3.6 at .% Yb could be accommodated with essentially no disruption of the $(d–d)$ structure, while 2.4 at .% Nd and 2.7 at .% Gd resulted in frequent twinning. Sm-zirconolite (9 at .% Sm) yields an $(r)^4$ structure and at
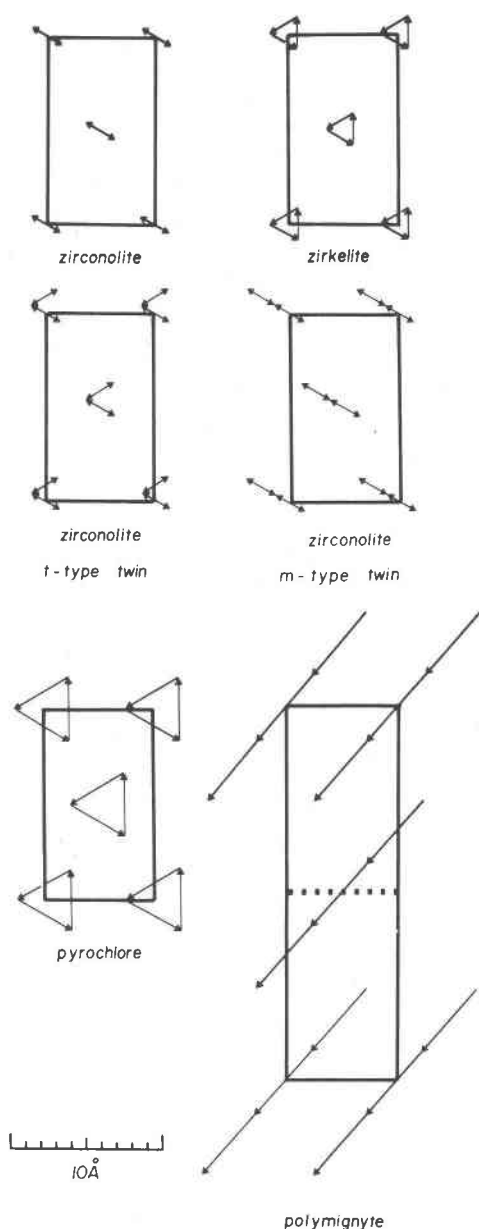
Table 2. Modular stacking sequences for zirconolite and its polytypes

Polytype	Unit SV Displacement (Å)	Modular Stacking Sequence	Crystallographic Repeat
Zirconolite	2.1	... d(-dd)-d ...	(-dd)
Zirkelite	2.1	... t(ttt)t ...	(t)³
Pyrochlore	2.1	... 2t(2t2t2t)2t ...	(2t)³
Zirconolite (m-type twin)	2.1	... d-dd m d-dd ... or ... d-dd m -dd-d ...	
Zirconolite (t-type twin)	2.1	... d-dd t d-dd ... or ... d-dd t -dd-d ...	
Polymignyte	5.5	... m(mmm)m ...	(m)³

Fig. 9. Stacking vector diagrams for zirconolite, zirkelite, pyrochlore and polymignyte. Zirconolite containing t-type and m-type twin boundaries are also shown.

appropriate concentrations other REE-doped zirconolites could behave similarly.

Conclusion

In this paper we have attempted to characterize zirconolite and its related structures in a manner which not only simplifies their description but also assists in our understanding of their microstructural properties. The modular concept is completely analogous to that used to describe mica polytypes and its success may be gauged from its ability to predict the likely topography of hettotypes, some of which have now been identified. Indeed such an approach could usefully be applied to any structure which may be divided into layers with (pseudo) hexagonal symmetry. (For example, the alunite/crandallite structures also contain HTB layers and several unidentified specimens remain (Blount, 1974; Cowgill et al., 1963). It is not unreasonable to suggest that some of these may arise from mimetic twinning).

The immediate interest in zirconolite stems from its inclusion in SYNROC (Ringwood et al., 1981). The means by which α-emitting radwaste is incorporated in the ceramic will profoundly influence the process of metamictization. In particular, theoretical models of radiation damage mechanisms which assume true diadochy must be regarded with suspicion; although such methods predict the correct bulk properties of the metamict material they will provide an unrealistic description of its microstructural characteristics.
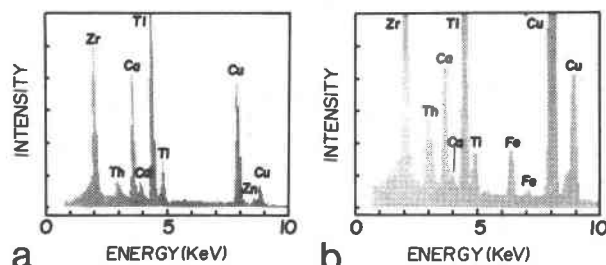

Fig. 10. Energy dispersive X-ray spectra for (a) zirconolite (nominal composition $Ca\ Th_{0.2}\ Zr_{0.8}\ Ti_2O_7$) and (b) zirkelite ($Ca_{0.8}\ Th_{0.2}\ Zr\ Ti_{0.8}\ Fe_{0.2}O_7$). Note the differences in the relative intensities of the Zr, Ca, Th and Ti peaks. These spectra should be compared with those of the other pseudotypes pyrochlore and polymigmyte (Fig. 17).
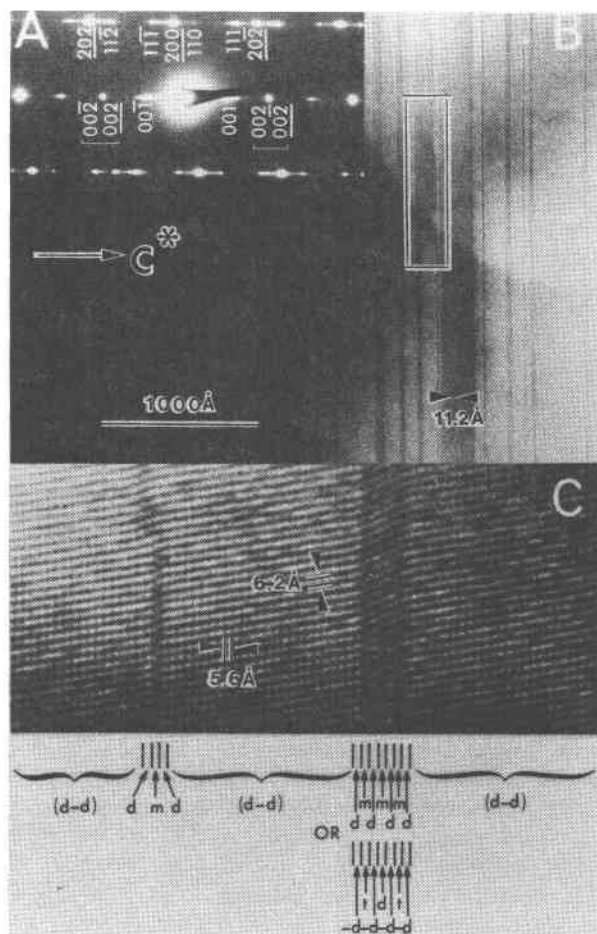
Fig. 11. A twinned (*d–d*) crystallite in the $Ca_{0.6}$ $Sm_{0.4}$ $ZrNb_{0.4}$ $Mg_{0.4}$ $Ti_{1.2}O_7$ formulation. A. SAD pattern indexed in terms of the $[010]_c$ reflections (underlined) and the $[110]_c$ reflections. B. Low magnification image showing the freqency of twinning. The squared area contains three spacings of ~22.4Å; these may be due to the $(r)^4$ superstructure. C. Higher magnification image of some twin boundaries. At the available resolution it was not possible to unequivocally label the modular staking sequences.

Acknowledgments
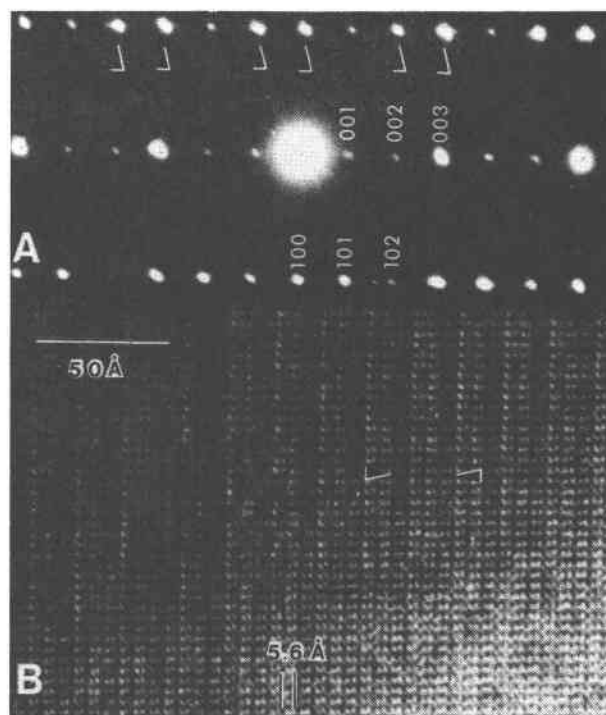
Fig. 12. A "perfect" crystallite of zirkelite with the bulk composition $Ca_{0.8}$ $Th_{0.2}$ Zr $Ti_{0.8}$ $Fe_{0.2}O_7$. A. SAD pattern indexed in terms of the trigonal axial setting. The intense pairs of second order reflections are arrowed. B. High resolution image showing the regularity in contrast across the modular (5.6Å wide) units. Contrast periodicity is consistent with a trimodular repeat.
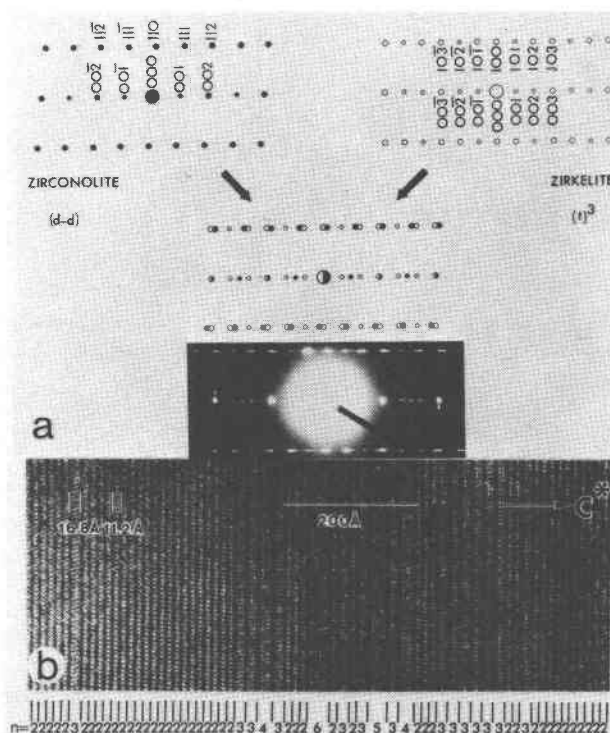

Fig. 13. Zirkelite of bulk composition $Ca_{0.8}Th_{0.2}Zr$ $Ti_{0.8}$ $Fe_{0.2}O_7$. (a)$[110]_c$ diffraction pattern of crystal containing coherent intergrowths between the (*d–d*) and $(t)^3$ structures. (b) High resolution image interpreted in terms of n in the polytype formula $(r)^n$. The 16.8Å repeat corresponds to the $(001)_c$ spacing of the $(t)^3$ type while the 11.2Å fringes are due to the $(001)_c$ spacing of the (*d–d*) aristotype.

Table 3. Microstructural characteristics for a variety of zirconolite-like formulations.

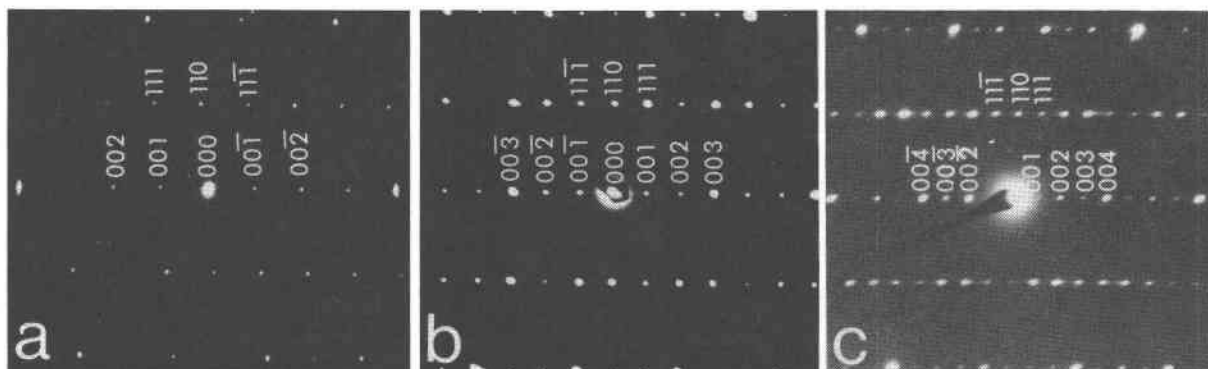| Bulk Formulation	Preparative Details	Redox Conditions	Constituents Identified
* $CaZrTi_2O_7$	Cold pressed and sintered 1400°C for 16 hr under CO/CO_2	Reducing	Zirconolite + Perovskite
** $CaZr_{0.96}Ti_{2.04}O_7$	Cold pressed and sintered 1450°C for 3 days	Oxidizing	Zirconolite
** $CaZr_{1.04}Ti_{1.96}O_7$	Cold pressed and sintered 1450°C for 3 days	Oxidizing	Zirconolite
$CaZrTi_{1.70}Al_{0.30}O_{6.7}$	5kbar, 1250°C, ½hr in Pt tube	Reducing	"Perfect" zirconolite and twinned zirconolite
$CaZrTi_{1.70}Al_{0.30}O_{6.7}$	5kbar, 1300°C, ½hr in Pt tube	Reducing	"Perfect" and twinned zirconolite.
$CaZrTi_{1.70}Al_{0.30}O_{6.7}$	5kbar, 1400°C, ½hr in Pt tube	Reducing	"Perfect" and twinned zirconolite. Perovskite + disordered cubic fluorite phase (stabilized ZrO_2).
$Ca_{0.9}Mn_{0.1}ZrTi_2O_7$	5 kbar, 1400–1450°C, 1 hr in Pt tube.	Reducing	Zirconolite
$Ca_{0.6}Mn_{0.4}ZrTi_2O_7$	5kbar, 1400–1450°C, 1 hr in Pt tube.	Reducing	Zirconolite
** $Ca_{0.87}Nd_{0.26}Zr_{0.87}Ti_2O_7$	Cold pressed and sintered 1410°C/4 days followed by 1440°C/2 days.	Oxidizing	Mostly perfect zirconolite. Some SAD had weak reflections indicative of an $(r)^4$ polytype.
** $Ca_{0.85}Gd_{0.30}Zr_{0.85}Ti_2O_7$	Cold pressed and sintered 1410°C/3 days.	Oxidizing	Mostly perfect zirconolite + some twinned zirconolite.
** $Ca_{0.8}Yb_{0.4}Zr_{0.8}Ti_2O_7$	Cold pressed and sintered 1400°C/4 days.	Oxidizing	Perfect zirconolite (A single crystallite containing one stacking fault was observed).

Fig. 14. Diffraction patterns of three $(r)^n$ structures recorded in the $[110]_c$ zone: (a) (d–d) aristotype (Ca Zr Ti$_2$O$_7$); (b) $(t)^3$ hettotype (Ca$_{0.77}$ Th$_{0.24}$ ZrTi$_{1.5}$ Al$_{0.5}$ O$_7$); (c) $(r)^4$ hettotype (Ca$_{0.5}$ Sm Zr$_{0.5}$Ti$_2$O$_7$).

Table 3. *(Cont.)*

Bulk Formulation	Preparative Details	Redox Conditions	Constituents Identified
$Ca_{0.5}SmZr_{0.5}Ti_2O_7$	5kbar, 1450°C, 1 hr in Pt tube	Reducing	Twinned zirconolite; SAD invariably contain diffuse $(r)^4$ polytype reflections. Also some pyrochlore.
$Ca_{0.6}Sm_{0.4}ZrNb_{0.4}Mg_{0.4}Ti_{1.2}O_7$	5kbar, 1500°C, 1 hr in Pt tube.	Reducing	Mixture of perfect zirconolite and twinned zirconolite
$CaTh_{0.2}Zr_{0.8}Ti_2O_7$	5kbar, 1350°C, 1 hr in Pt tube.	Reducing	Perfect zirconolite and twinned zirconolite. Also a little pyrochlore.
$Ca_{0.77}Th_{0.24}ZrTi_{1.5}Al_{0.5}O_7$	5kbar, 1450°C, 1 hr in Pt tube.	Reducing	Mostly perfect zirkelite + some twinned zirkelite.
$Ca_{0.7}Th_{0.3}ZrTi_{1.7}Mg_{0.3}O_7$	5kbar, 1450°C, 1 hr in Pt tube.	Reducing	Some crystallites were twinned but most were perfect zirkelite.
$Ca_{0.8}Th_{0.2}ZrTi_{1.8}Fe_{0.2}O_7$	5kbar, 1350°C, 1 hr in Pt tube.	Reducing	Coherent intergrowths of zirconolite, zirkelite and $(r)^n$, n>3 polytypes
$Ca_{0.7}Th_{0.3}ZrTi_{1.7}Fe_{0.3}O_7$	5kbar, 1350°C, 1 hr in Pt tube.	Reducing	Polymignyte
$CaU_{0.25}Zr_{0.75}Ti_2O_7$	5kbar, 1400°C, 1 hr in Pt tube.	Reducing	Mixture of twinned and perfect zirconolite. Some pyrochlore.
$CaU_{0.5}Zr_{0.5}Ti_2O_7$	5kbar, 1400°C, 1 hr in Pt tube.	Reducing	Pyrochlore
$CaU_{0.75}Zr_{0.25}Ti_2O_7$	5kbar, 1400°C, 1 hr in Pt tube.	Reducing	Pyrochlore
$CaUTi_2O_7$	5kbar, 1400°C, 1 hr in Pt tube	Reducing	Pyrochlore

*   *Specimens provided by AAEC (Lucas Heights)*
**   *Specimens provided by CSIRO (Division of Materials Science)*
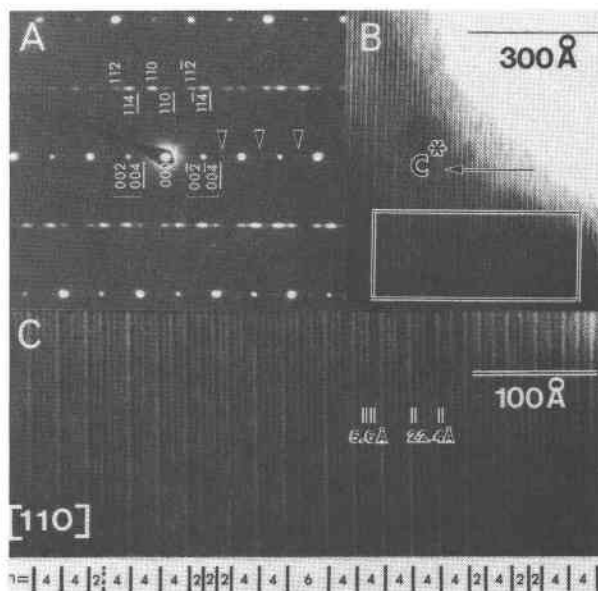
Fig. 15. "Zirconolite" of bulk formulation $Ca_{0.5}$ Sm $Zr_{0.5}Ti_2O_7$. A. SAD pattern indexed in terms of the $(r)^4$ structure. The arrows indicate diffuse reflections (visible in the original) which correspond to the $00l$, $l \neq 2r$ planes of the $(r)^4$ type. B. Low magnification image illustrating the extensive intergrowth. Note that only a bimodular repeat is apparent at the thin edge of the crystal. C. Higher magnification image of outlined area in B. The lattice image is interpreted as lamallae of various r in $(r)^n$.
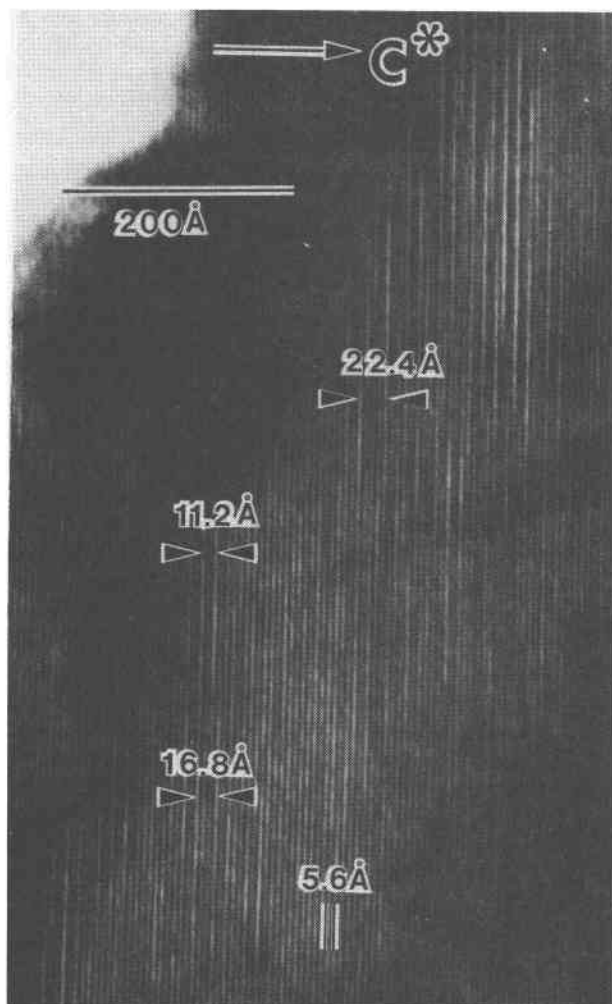
Fig. 16. An imperfectly ordered aluminozirconolite crystallite prepared at 1400°C. The lattice image consists of a complex arrangement of ordered $(r)^n$ superstructures. The 11.2Å, 16.8Å, and 22.4Å supercells correspond to the $(d-d)$, $(r)^3$ and $(r)^4$ structures respectively. The 5.6Å lattice fringes are consistent with the $d(002)$ spacing of $(d-d)$ zirconolite, (i.e., the modular thickness).

Fig. 17. (a), (b) X-ray spectre and $[110]_{cu}$ diffraction pattern of pyrochlore with bulk composition Ca $U_{0.5}Zr_{0.5}Ti_2O_7$). (c), (d) X-ray spectra and $[100]_o$ diffraction pattern for polymignyte of bulk composition $Ca_{0.7}Th_{0.3}Zr Ti_{0.7}Fe_{0.3}O_7$. Note the correspondence between the fluorite subcell refections in the SAD patterns of pyrochlore and polymignyte.

References

Bagshaw, A. N. (1976). Diverse structures based on the Fd3m space group. Zeitschrift für Kristallographie, 144, 53–63.

Blake, G. S. and Smith, G. F. (1913). On varieties of zirkelite from Ceylon. Mineralogical Magazine, 16, 309–316.

Blount, A. M.(1974). The crystal structure of crandallite. American Mineralogist, 59, 41–47.

Borodin, L. S., Bykova, A. V., Kapitonova, T. A. and Pyatenko, Yu. A. (1961). New data on zirconolite and its niobuim variety. Doklady Akademiya Nauk SSSR, 134, 1022–1024 (not seen; abstracted from Mazzi and Munno, 1983).

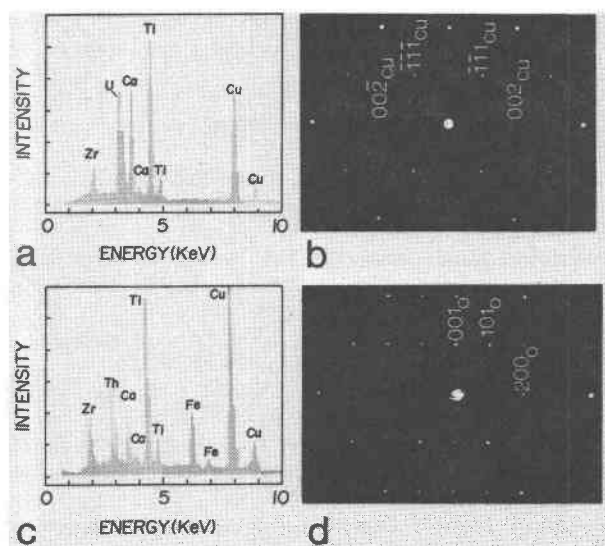Cowgill, U. M., Hutchison, G. E., and Joehsuu, O. (1963). An apparently triclinic dimorph of crandallite from a tropical swamp sediment in El Peten, Guatemala. American Mineralogist, 48, 1144–1153.

Darriett, B., Rat, M., Galy, J., and Haganmuller, P. (1971). Sur quelques nouveaux pyrochlores des systems MTO_3-WO_3 et MOT_3-TeO_3. Materials Research Bulletin, 6, 1305–1316.

Gaertner, H. R.(1930) die Kristallstrukturen von Loparitte und Pyrochlor. Neues Jahrbuch für Mineralogie, 61, 1–30.

Gatehouse, B. M., Grey, I. E., Hull, R. J., and Rossell, H. J. (1981). Zirconolite, Ca Zr_xTi_{3-x} O_7; Structure refinements for near-end-member compositions with x = 0.85 and 1.30. Acta Crystallographica, B37, 306–312.

Hogarth, D. D. (1977). Classification and nomenclature of the pyrochlore group. American Mineralogist, 62, 403–410.

Hutchison, J. L., Barry, J. C., Segall, R. L., and White, T. J. (1983). High resolution lattice images of zirconolite. Proceedings of EMAG 1983 Conference, Institute of Physics Conference Series No.68, p. 403–406. Institute of Physics, Guildford.

Hyde, B.G., Andersson, S., Bakker, M., Plug, C. M., O'Keeffe, M. (1979). The (twin) composition plane as an extended defect and structure-building entity in crystals. Progress in Solid State Chemistry, 12, 273–327.

Kesson, S. E., Sinclair, W. J., Ringwood, A. E. (1984). Solid solution limits in SYNROC zirconolite. Nuclear and Chemical Waste Management, in press.

Lima-de-Faria, J. (1958). Heat treatment of metamict euxenites, polymignytes, yttrotantalites, samarskites, pyrochlores and allanites. Mineralogical Magazine, 31, 937–942.

Mazzi, F. and Munno R. (1983). Calciobetafite (new mineral of the pyrochlore group) and related minerals from Campi Flegrei, Italy; crystal structures of polymigntye and zirkelite: comparison with pyrochlore and zirconolite. American Mineralogist, 68, 262–276.

Nyman, H. (1983). A relation between the structures $Ce_{24}Co_{11}$, Ru_7B_3 and pyrochlore. Journal of Solid State Chemistry, 49, 263–268.

Nyman, H., Andersson, S., Hyde, B. G., and O'Keeffe, M. (1978). The pyrochlore structure and its relatives. Journal of Solid State Chemistry, 26, 123–131.

O'Keeffe, M. and Hyde, B. G. (1980). Plane nets in crystal chemistry. Philosophical Transactions of the Royal Society of London, 295, 553–623.

Pannetier, J. and Lucas, J. (1970). New description of the pyrochlore structure $Cd_2Nb_2O_6S$. Materials Research Bulletin, 5, 797–805.

Pyatenko, Yu. A. and Pudovkina, Z.V. (1964). The lattice metric of $CaZrTi_2O_7$ crystals. Kristallografiya, 9, 98–100.

Ringwood, A. E., Oversby, V. M., Kesson, S. E., Sinclair, W., Ware, N., Hibberson, W., and Major, A. (1981). Immobilization of high-level nuclear reactor wastes in SYNROC: A current appriasal. Nuclear and Chemical Waste Management, 2, 287–305.

Rossell, H. J. (1980). Zirconolite—a fluorite-related superstructure. Nature, 283, 282–283.

Shannon, R. D. and Prewitt, C. T. (1969). Effective ionic radii in oxides and fluorides. Acta Crystallographica, B25, 925–946.

Sinclair, W. J. (1982). Aspects of Crystal Chemistry. Ph.D. Thesis, Australian National University, Canberra.

Sleight, A. W. (1968). New ternary oxides of mercury with the pyrochlore structure. Inorganic Chemistry, 7, 1704–1708.

Smith, J. V., Yoder, H. S. (1954). Experimental and theoretical studies of the mica polymorphs. Mineralogical Magazine, 31, 209–235.

Strukturbericht (1914) 2, 60. Leipzig.

Subramanian, M. A., Aravamudan, G., Subba Rao, G. V. (1983). Oxide pyrochlores—a review. Progress in Solid State Chemistry, 15, 55–143.

Thompson, J. B. Jr. (1981). Polytypism in complex crystals: contrasts between mica and classical polytypes. In A. Navrotsky and M. O'Keeffe, Eds., Structure and Bonding in Crystals Vol. II, p. 167–196. Academic Press. New York.

White, T. J., Segall, R. L., Barry, J. C., and Hutchison, J. L. (1984). Polytypic behaviour of zirconolite. Proceedings of the Royal Society, (London), A392, 343–358.

Yagi, K., Roth, R. S. (1978). Electron-microscope study of the crystal structures of mixed oxides in the systems Rb_2O–Ta_2O_5, Rb_2O–Nb_2O_5 and K_2O–Ta_2O_5 with composition ratios near 1:3 I. Stacking characteristics of MO_6 layers. Acta Crystallographica, A34, 765–773.